frontiers | Frontiers in Marine Science

TYPE Original Research
PUBLISHED 13 March 2023
DOI 10.3389/fmars.2023.1111133

OPEN ACCESS

EDITED BY
Dong Feng,
Shanghai Ocean University, China

REVIEWED BY
Rui Yang,
Qingdao Institute of Marine Geology (QIMG), China
Xiting Liu,
Ocean University of China, China
Claudio Argentino,
UiT The Arctic University of Norway, Norway

*CORRESPONDENCE
Daidai Wu
wudd@ms.giec.ac.cn
Ping Yin
1419685757@qq.com

SPECIALTY SECTION
This article was submitted to Marine Biogeochemistry, a section of the journal Frontiers in Marine Science

RECEIVED 29 November 2022
ACCEPTED 27 February 2023
PUBLISHED 13 March 2023

CITATION
Sun T, Wu D, Wu N and Yin P (2023) The effects of organic matter and anaerobic oxidation of methane on the microbial sulfate reduction in cold seeps. *Front. Mar. Sci.* 10:1111133. doi: 10.3389/fmars.2023.1111133

The effects of organic matter and anaerobic oxidation of methane on the microbial sulfate reduction in cold seeps

Tiantian Sun[1,2], Daidai Wu[3]*, Nengyou Wu[1,2] and Ping Yin[1,2]*

[1]Qingdao Institute of Marine Geology, China Geological Survey, Ministry of Natural Resources, Qingdao, China, [2]Laboratory for Marine Geology, Qingdao National Laboratory for Marine Science and Technology, Qingdao, China, [3]Guangzhou Institute of Energy Conversion, Chinese Academy of Sciences, Guangzhou, China

Cold seep sediments are dominated by intensive microbial sulfate reduction coupled to anaerobic oxidation of methane. However, the contribution proportion between this process and the role of organic matter has remained enigmatic. Here, pore water data combined with PROFILE model, fluxes of sulfate and methane concentration calculated from Fick's first law, and $\delta^{34}S_{SO4}$ and $\delta^{18}O_{SO4}$ of pore water sulfate were studied to reconstruct co-occurring microbial organoclastic sulfate reduction and anaerobic oxidation of methane coupled with sulfate reduction in methane seep sediments collected from South China Sea. The sulfate concentration profiles of C9 and C14 in Qiongdongnan Basin generally show quasilinear depletion with depth. Reaction-transport modeling provided close fits to concentration data. $\delta^{18}O_{SO4}$ and $\delta^{34}S_{SO4}$ increase fastest with sediment depth above 400 cmbsf and slowest below that depth. The values of methane flux are always lower than those of total sulfate reduction of sulfate diffusive flux at GC-10, GC-9, GC-11 and HD319 sites in Taixinan Basin. Besides, positions of sulfate methane transition zone in all study sites are approximately ~400 to 800 centimeters below seafloor. These results showed that microbial sulfate reduction in sediments is mainly controlled by intense anaerobic oxidation of methane, but there is a certain relationship with organic matter metabolism process. This emphasizes that traditional redox order of bacterial respiration is highly simplified, where, in sediments such as these seeps, all of these microbial sulfate reduction processes can occur together with complex couplings between them.

KEYWORDS

methane seepage, anaerobic oxidation of methane, microbial sulfate reduction, Organoclastic Sulfate Reduction, Qiongdongnan Basin, Taixinan Basin

1 Introduction

In the early diagenesis of sediments, pore water in sediment close to the seafloor is rich in sulfate due to the downward diffusion and infiltration of high concentration of sulfate in the ocean. Organoclastic sulfate reduction (OSR): $2(CH_2O) + SO_4^{2-} \rightarrow 2HCO_3^- + H_2S$ (Berner et al., 1985; Boetius et al., 2000) and anaerobic oxidation of methane coupled with sulfate reduction (AOM-SR): $SO_4^{2-} + CH_4 \rightarrow HCO_3^- + HS^- + H_2O$ (Masuzawa et al., 1992; Knittel and Boetius, 2009) are important microbial sulfate reduction (MSR) pathways in sediments, which play a vital role in the sulfur and carbon cycles in marine sediments. Those with highly active organic matter with sulfate reduction occur in the sulfate reduction zone (SRZ). Below the SRZ lies the sulfate-methane transition zone (SMTZ), a zone where methane and sulfate would be exhausted. The upward diffusion of methane in sediment directly controls the gradient of sulfate change in pore water and the depth position of the SMTZ. Generally, the greater the upward diffusion flux of methane, the more intense the AOM reaction, resulting in a shallower SMTZ depth (Borowski et al., 1996; Borowski et al., 1999). Borowski et al. (1999) conducted a systematic study on the change in sulfate concentration in pore water during the Deep Sea Drilling Project (DSDP) and Ocean Drilling Program (ODP) stations on the continental margins around the world and found that the SMTZ depth of most gas hydrate occurrence areas and cold seeps are less than 50 m, with an average of 20 m. In the area where hydrate occurs, the content of SO_4^{2-} in pore water decreases rapidly due to strong AOM, which makes the SMTZ in sediments shallow. Therefore, linear and steep sulfate profile gradients and shallow SMTZ positions are signs of strong methane flux and possible existence of AOM-SR (Borowski et al., 1996; Borowski et al., 2000; Wu et al., 2013).

Most geochemical and microbiological studies point to AOM-SR as the dominant sink for methane (up to 90%) in cold seep sediments (Knittel and Boetius, 2009). However, the proportion of this process has remained enigmatic. For methane seep sediments under different environmental settings, the proportion of sulfate consumed in pore water by OSR and AOM-SR differs. For example, only 50% of sulfate diffused downward from pore water of the Cariaco Trench basin in Venezuela is consumed by AOM (Reeburgh, 1976). 61-89% of the sulfate in the bottom sediments of the Kattegat Strait and Skagrak Strait is consumed by AOM (Jørgensen, 1992). Besides, Egger et al. (2018) conducted a detailed study on sulfate and methane fluxes in the SMTZ from the worldwide. They concluded that OSR consumed more than 40% of sulfate in the SMTZ. Jørgensen et al., (2019b) studied the content of methane and sulfate and their reaction rates in pore water at several sites along the Danish coast and found that about 14-59% of sulfate near the SMTZ was consumed through OSR. These studies have helped demonstrate the important role of OSR in the MSR process within sedimentary systems under the background of methane seeps, even in the presence of AOM. However, many questions remain. There is still enigmatic on the ratio of sulfate consumed by anaerobic oxidation of methane (AOM) and sulfate consumed by organic matter-driven MSR when both processes occur, as well as their influencing control factors.

Separating the contributions of OSR and AOM-SR to the overall sedimentary sulfur cycle has been challenging but has benefited from recent advances in isotope biogeochemistry. Stable carbon isotopes have been vastly used to address these processes. Recently, the sulfur and oxygen isotopes in dissolved sulfate ($\delta^{34}S_{SO4}$ and $\delta^{18}O_{SO4}$) may be a diagnostic tool for tracking the pathways of sulfate reduction by methane or other organic compounds (Böttcher et al., 1998; Gilad et al., 2013; Deusner et al., 2014; Gilad et al., 2014; Chen et al., 2022). Metabolic processes distinguish light and heavy isotopologues, and the gradual enrichment of heavy isotopes observed in the residual sulfate pool can trace this activity. The overall rate of MSR itself is related to the relative chemical balance of the several main intracellular steps, each step is reversible, and the branching points generated in the cell itself will respond to changes in environmental conditions (Wing and Halevy, 2014; Santos et al., 2015). A fast increase in $\delta^{18}O$ of sulfate relative to its $\delta^{34}S$ suggests there is a high rate of back-reaction and equilibration of oxygen isotopes in intermediate-valence-state-sulfur species with water, and thus a slower overall rate of MSR (Chen et al., 2022). Two other processes impact the sulfur isotope fractionation observed in sediments, the disproportionation of external sulfur intermediates and microbial sulfide oxidation, and the observed sulfur isotopic composition of sulfate may be due to a combination of all three processes (Jørgensen et al., 2019a; Pellerin et al., 2019). This relationship has been investigated in pure culture experiments (Canfield et al., 2006), batch culture experiments using natural populations (Stam et al., 2011) and calculated *in situ* using pore fluids profiles (Aharon and Fu, 2000; Gilad et al., 2013). The drilling research of Deep Sea Drilling Project (DSDP) Leg 11 and Leg 76 also shows that methane intensity affects the stable S and O isotope values of sulfate in sedimentary pore water, which often shows a series of geochemical anomalies in depth profiles (Borowski et al., 1996; Borowski et al., 2000).

Here, we compare and analyze the pore water composition and PROFILE model of six sedimentary sites collected from the Qiongdongnan Basin and the Taixinan Basin, respectively, in the South China Sea to study OSR and AOM-SR of two important microbial sulfate reduction in cold seep sediments and the location of SMTZ that can be used to indicate the intensity of methane seepage. Sulfate and methane concentration gradients into SMTZ are used to estimate sulfate reduction rates and AOM rates. Combined with $\delta^{34}S_{SO4}$ and $\delta^{18}O_{SO4}$ of pore water sulfate to help evaluate whether OSR accounts for a certain proportion during AOM-SR process. We provide strong evidence for the co-existence of OSR and AOM under the background of cold seeps, and propose that the intensity of methane seepage significantly influence mechanisms on the $\delta^{34}S_{SO4}$ and $\delta^{18}O_{SO4}$ of pore water. In the process of microbial sulfate reduction, $\delta^{34}S_{SO4}$ and $\delta^{18}O_{SO4}$ in the residual sulfate are also affected by the disproportionation of external sulfur intermediates and the oxidation of microbial sulfide.

2 Study area

The South China Sea is one of the largest marginal seas in the low-latitude area of the Western Pacific Ocean. It is located at the intersection of Eurasian plate, Pacific plate and India-Australia plate (Taylor and Hayes, 1983). There are various structural landforms or geological bodies on the continental slope, such as deep troughs, submarine plateaus, continental slope platforms, steep submarine slopes and submarine valleys. From the seismic profile of gas hydrate distribution areas in the typical passive continental margin, most of the seafloors are developed with abundant faults and/or fold structures, and the hydrate enrichment zone is primarily concentrated in the sedimentary layer near or above the major faults (Hu et al., 2020). The study area includes two areas in the northern slope of the South China Sea (Qiongdongnan and Taixinan), with the water depth ranging from ~700 to ~ 2000 meters (see Figure 1). According to the survey of marine resources, clear undersea simulated reflectors (BSRs) have been found in Xisha Trough, Taixinan Basin, Shenhu and Dongsha areas, Qiongdongnan Basin, which to a large extent indicates that there are huge potential sources of natural gas hydrates in the northern South China Sea (Yao, 1998).

The GC-9, GC-10, GC-11 and HD319 sites are located in the Taixinan basin in the southwest of Taiwan Province (Figure 1). The abundant terrestrial clastic rocks derived from Southern China and the Indochina Peninsula have resulted in Neogene sediment deposits up to ~10 km thick at the center of Taixinan Basin. The thick stratigraphic deposits and intense hydrocarbon generation and expulsion processes of the deep source kitchens have led to high fluid activity, forming a series of NE-trending basin that are rich in oil and gas, with widely distributed mud volcanoes, mud diapirs, gas chimneys, and submarine cold seeps (Schnürle et al., 2011). Moreover, gas seepages and associated cold seeps have been confirmed *via* multibeam profiles and *in situ* ROV observations. During the R/V SONNE 177 cruise in 2007, a widely distributed seep carbonate crust called Jiulong Methane Reef was found in the deep waters of the Taixinan Basin, indicating extensive paleo-methane seep events in this area (Suess et al., 2005; Han et al., 2008).

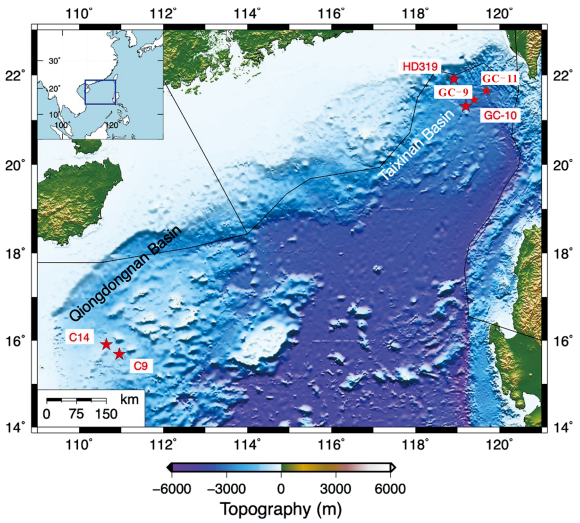

FIGURE 1
Map of study sites and locations in the northern South China Sea. Rectangle boxes denote study areas, which includes the Qiongdongnan basin and Taixinan basin.

Sites C9 and C14 are located in southwest Qiongdongnan Basin (Figure 1). The Qiongdongnan Basin, located on the northwestern continental slope of the SCS, contains a Cenozoic sedimentary succession of up to 12 km in thickness and is suggested to have great hydrocarbon and gas hydrate potential (Zhu et al., 2009; Shi et al., 2013; Zhang et al., 2018). A large number of seabed pockmarks, mounds and acoustic blanking reflections related to submarine fluid flow together with indicators of shallow gas hydrate occurrence have been reported in the western Qiongdongnan Basin (Sun et al., 2011; Luo et al., 2014). In 2015, "Haima cold seeps" were discovered in the southern Qiongdongnan Basin during ROV surveys launched by the Guangzhou Marine Geological Survey. Piston and push coring processes also recovered gas hydrates and authigenic carbonate rocks from subsurface sediments at seepage sites in the Qiongdongnan Basin (Liang et al., 2017).

3 Materials and methods

3.1 Data

This study primarily utilized public and published data; reference sources are provided for all the data. The concentration of major components (SO_4^{2-}, Ca^{2+}, DIC) and ^{34}S isotope value of sulfate in pore water in the Qiongdongnan Basin is from the data of Luo et al. (2013), while the ^{18}O isotope value of sulfate is from the data of Luo et al. (2014); The concentration of CH_4 and major components (SO_4^{2-}, Ca^{2+}, H_2S, TA, Sr^{2+}, Mg^{2+}, Ba^{2+}, Mn^{2+}) in pore water in the Taixinan Basin is from the data of Wu et al. (2010); Wu et al. (2013). However, these data have not previously been used for the same purpose as this study. The number of complete datasets available is limited, and only four are listed here. The geographic locations of the six sampling sites are shown in the figure (Figure 1). Names and coordinates of all sites are given in Table 1 together with other key parameters (water depth, core length, and references).

3.2 Numerical modeling

The measured concentration gradient of pore water was used to calculate the net production or net consumption rate of the primary elements (SO_4^{2-}, CH_4, Ca^{2+}, H_2S, DIC) in the sediment pore water from the four stations (stations C9, C14, GC-10, and HD319) and the resulting vertical flux. SMTZ is a zone with unclear boundaries, especially on the continental shelf sediments rich in organic matter. It usually occurs within a few meters of shallow surface sediments. The methane profile extends to the sulfate reduction zone (Schmaljohann, 1996; Piker et al., 1998; Jørgensen et al., 2004). In this study, a reaction transport model was used to determine the depth range when the net methane consumption rate (AOMR) and sulfate reduction rate (SRR) increase. It was assumed that the

TABLE 1 Coordinates, water depth and core length at the sediment stations sampled on the northern South China Sea; bsf is below sea floor.

Station	Latitude (N)	Longitude (E)	Core length (cm bsf)	Water depth (m bsf)	References from
C9	15°41.032′	110°57.246′	760	829	(Luo et al., 2014)
C14	15°54.507′	110°38.607′	670	840	(Luo et al., 2014)
GC-10	21°18′27″	119°11′49″	937	3008	(Wu et al., 2010)
GC-9	21°18′27″	119°11′50″	850	3009	(Wu et al., 2013)
GC-11	21°18′29″	119°11′58″	730	3008	(Wu et al., 2013)
HD319	21°54′48″	118°54′47″	730	1730	(Wu et al., 2010)

Sampling method and survey ship description: GC, gravity coring (Taiyang), HD, large gravity piston coring (Haiyang IV).

system is in a stable state and only diffuses through molecules. This condition is consistent with the diffusion around the sediment SMTZ. The standard boundary condition used is the concentration of the main components in the pore water. These combined depth intervals were used to define the biogeochemical processes at the upper and lower boundaries of SMTZ and its surroundings, and are compared with the measured data.

The one-dimensional numerical model software PROFILE proposed by Berg et al. (1998) was used for simulation. The software first divides the sediment into any number of equally spaced blocks, and each block has a constant reaction rate. By selecting the simplest reaction rate distribution, the least square method was used to fit the best concentration curve of the data. The model conducts the F test for different solutes, ensuring the continuity of flux between regions and providing the solute flux.

According to previous research (Luo et al., 2013), sites C9 and C14 within 100 cmbsf are mainly controlled by OSR. Therefore, one-dimensional reaction-transport modeling of the pore water sulfate concentration profiles in Qiongdongnan was developed to estimate the net rates of sulfate reduction in subsurface sediments using the software PROFILE (Berg et al., 1998). The reaction rate was calculated in volume units of sediment per day (nmol cm^{-3} d^{-1}). The net reaction and net consumption per square meter per day during the interval are calculated in mmol m^{-2} d^{-1} based on the volume ratio within the interval of a determined depth. Considering the oxygen enrichment of the bottom seawater at these sites in this study, there may be biological disturbances in Taixinan Basin. Therefore, an unsteady-state scenario at GC-10, GC-9, GC-11 and HD319 sites can be supported by Fick's first law. This procedure assumed that sulfate transport only occurs *via* molecular diffusion. The assumption is largely consistent with the study sites where subsurface sediments are dominantly affected by sulfate or methane diffusion instead of advection as usually seen at methane seeps (Hu et al., 2020). Calibration of the diffusive coefficient with tortuosity was after the equation of Boudreau (1997). Here, the diffusion coefficient of sediment was calculated according to the porosity using the empirical equation of Iversen and Jørgensen (1993): $D_s = D_{sw}/[1 + 3(1-\Phi)]$.

The diffusion flux J was obtained by Fick's first law according to the pore water concentration profile (Schulz, 2006): $J = -\Phi D_s (dC/dx)$.

Here, Φ refers to the sediment porosity, set as 0.75 under stable conditions, see Wang et al. (2000). Ds is the diffusion coefficient of the whole sediment package after curve correction, C is the concentration of components in pore water, x is depth, and dc/dx is the vertical concentration gradient. This study assumed that the average pH value of sediment for all research stations was 7.5, and the bottom water temperature was uniformly set as 5 °C (refer to (Jin and Wang, 2010). The diffusion coefficients D_{SW} (m^2s^{-1}) of pore water components (SO_4^{2-}, CH_4, Ca^{2+}, DIC) at the relevant temperature and salinity were taken from Schulz (2006) and corrected for the set temperature and salinity. The D_{SW} values (m^2s^{-1}) of CH_4, SO_4^{2-}, and Ca^{2+} were 9.0 $x10^{-10}$, 5.7$x10^{-10}$, and 4.3$x10^{-10}$, respectively. For DIC, according to the set temperature of 5°C, the D_{SW} values of CO_3^{2-} and HCO_3^- were 5.04$x10^{-10}$ and 6.09$x10^{-10}$ respectively. The effective diffusion coefficients were 5.4$x10^{-10}$ and 5.565$x10^{-10}$, respectively.

4 Results and discussion

4.1 Microbial sulfate reduction in the pore water

We analysed 6 sediment cores, including 4 in Taixinan and 2 in Qiongdongnan, and all the geochemical data are shown in Table S1. The concentration profiles of SO_4^{2-}, CH_4, TA, DIC, H_2S and Ca^{2+}, Sr^{2+}, Mg^{2+}, $Mn^{2+}$and Ba^{2+} in the pore water of stations C9 and C14 in the Qiongdongnan Basin and GC-9, GC-10, GC-11 and HD319 in the Taixinan Basin are shown in Figure 2. The sulfate concentration profiles of C9 and C14 in Qiongdongnan Basin generally show quasilinear depletion with depth (Figure 2). Ca^{2+} concentration profiles in Qiongdongnan decreases sharply and then decreases slowly with depth. In contrast, DIC concentration profiles in Qiongdongnan generally increased with depth. Reaction-transport modeling provided close fits to the concentration data (Figure 2), which can be used to identify AOM and quantify the rates of AOM-SR (e.g., Jørgensen et al., 2019b).

Dissolved sulfate is the main electron acceptor available for the oxidation of organic matter and methane, and it is mainly supplied by diffusion from, or burial of, overlying seawater. Especially in the 0-100 cmbsf, rapid SO_4^{2-} consumption rates and concave-down

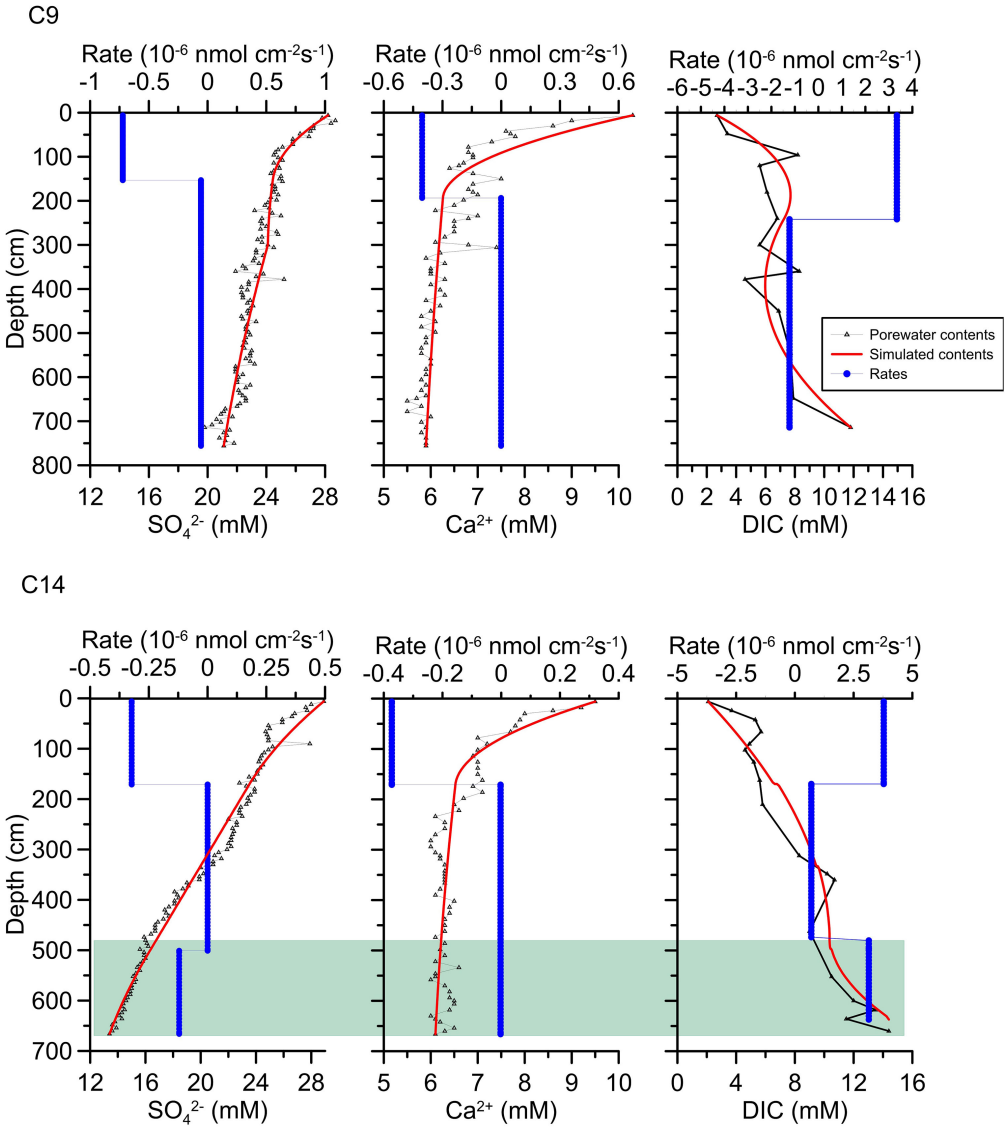

FIGURE 2
Depth profiles of pore water geochemical data for C9 and C14 sites. Black triangle with line indicates the measured concentration, red line represents the simulated concentration based on PROFILE model, and the blue line represents the net (production or consumption) reaction rate. Green shadow indicates the sulfate-methane transition zone.

curvatures at C9 and C14 sites, indicating that the microbial sulfate reduction is dominated by OSR in the uppermost sediments (Borowski et al., 1996; Hu et al., 2015; Miao et al., 2022). Jørgensen et al. (2001) showed that OSR was the most active in near-surface sediments, which was due to the high unstable organic load and sulfate flux at the sediment-water interface. Therefore, simulated OSR rates of C9 and C14 sites are $0.7*10^{-6}$ nmol cm^{-2} s^{-1} and $0.3*10^{-6}$ nmol cm^{-2} s^{-1} (Figure 2), which is relatively fast within 0-100 cmbsf. With easily degradable organic matter and sulfate being consumed, sulfate reduction rate declines, thereby resulting in less steep slopes for sulfate concentrations below 100 cmbsf. However, pore water concentration profiles of SO_4^{2-} and DIC and their reaction rate of the two sites are different below 500 cmbsf. The gradually increasing DIC concentration and slowly decrease in SO_4^{2-} consumption at C9 site are predominantly in response to OSR. For C14 site, SO_4^{2-} concentration display approximate linear decline below 500 cmbsf, and is accompanied by distinct increasing DIC concentration. Moreover, the sulfate reduction rate is $0.1*10^{-6}$ nmol cm^{-2} s^{-1} and DIC production reaction rate is $3.15*10^{-6}$ nmol cm^{-2} s^{-1} below 500 cmbsf. Compared with the sulfate reduction rate dominated by OSR at the bottom of C9 ($0.06*10^{-6}$ nmol cm^{-2} s^{-1}), it indicates that there may be additional sulfate consumption reaction and DIC production reaction at the bottom of C14. Previous studies suggested that OSR and AOM-SR co-occurrence in sediments can also result in a nearly linear change in the sulfate concentration profile (Malinverno and Pohlman, 2011). Considering the study area in Qiongdongnan Basin is located in pockmark area, it is speculated that there is probably dominated by OSR and AOM-SR

in the study sites of Qiongdongnan Basin. Based on the reaction equations of OSR and AOM-SR, Luo et al. (2013) distinguished the types of sulfate reduction reaction by using the diagram of the produced DIC versus consumed sulfate ratios after correcting for carbonate precipitation. Their results showed that the ratios were close to 2:1 at the bottom of C9, while were between 1.6:1 and 1:1 at the bottom of C14. Combined with the simulated rate data, it further suggests that MSR of C9 are predominantly in response to OSR, whereas the sulfate reduction below 500 cmbsf of C14 is affected by AOM-SR. The main sulfate reduction process of C14 is caused by varying proportions of contributions from OSR and AOM-SR. But due to the diversity of methane seepages activities, such as methane seepage activity in dormancy or declining period, some discriminant MSR (OSR or AOM-SR) proxies and the boundary between OSR and AOM-SR are missing in indicating certain methane seepages activities (Miao et al., 2022).

Sulfate concentration profiles at GC-10, GC-9, GC-11 and HD319 sites in Taixinan Basin do not follow the general trend of quasi-linear decrease. In the GC-10 site (Figure 3), SO_4^{2-} concentrations display near-seawater value above 400 cmbsf, and then approximately linearly decreases to the lower level at 750 cmbsf, where H_2S and TA reach the maximum value. Below 750 cmbsf, H_2S and TA gradually decreased while methane increased sharply. Based on the above indicators, It can be seen that the specific depth of the SMTZ in GC-10 to be approximately 700-800 cmbsf (Borowski et al., 1996). Similarly, the characteristics of

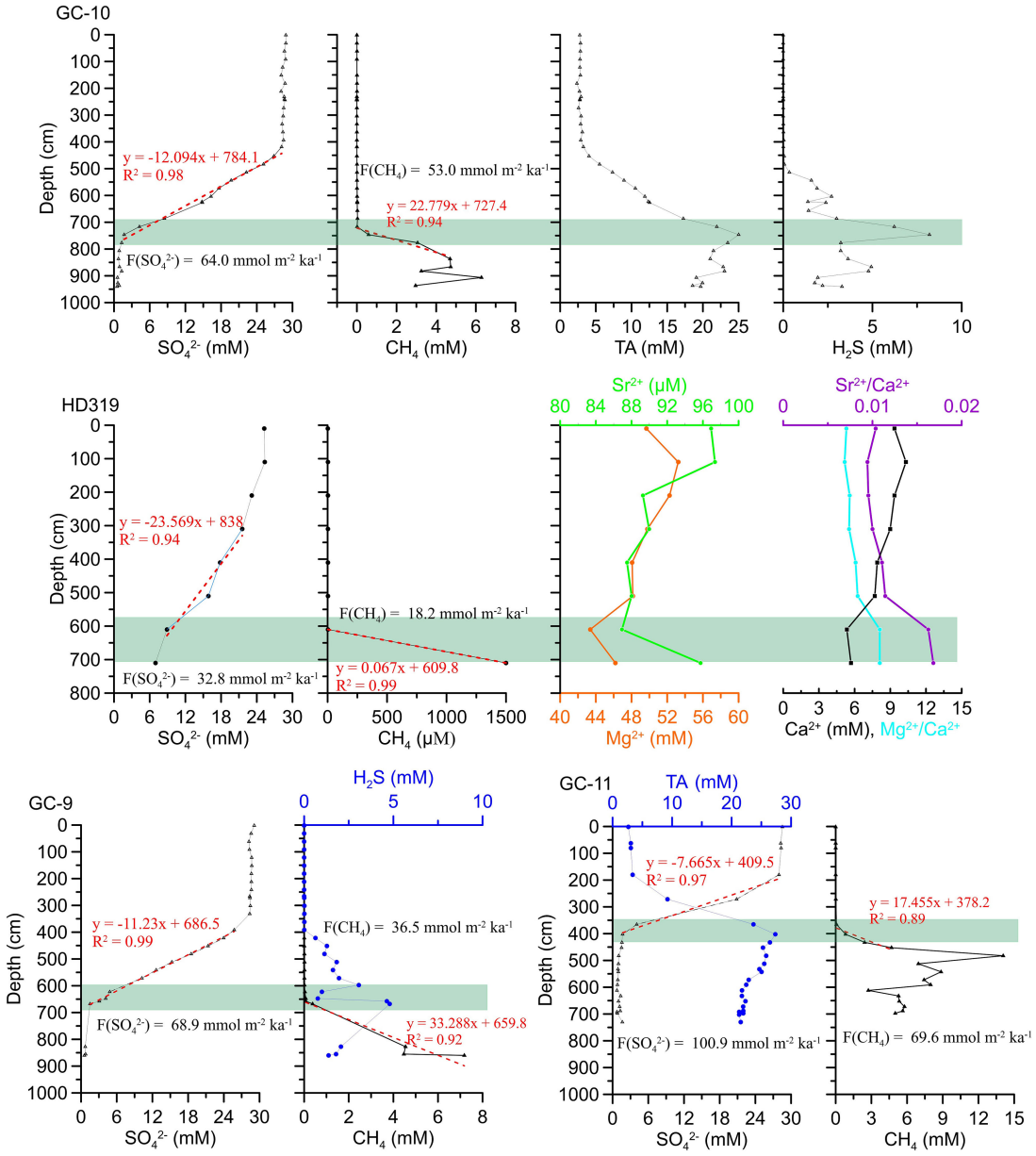

FIGURE 3
Depth profiles of pore water geochemical data for GC-9, GC-10, GC-11 and HD319 sites. Red dotted line represents CH_4 or SO_4^{2-} concentration linear fitting curve entering the sulfate-methane transition zone. Green shadow indicates sulfate-methane transition zone.

methane, SO_4^{2-}, H_2S and TA in pore water of stations GC-9 and GC-11 also have similar characteristics (Figure 3), it can be said that the SMTZ of GC-9 and GC-11 are 600-700 cmbsf and 350-450 cmbsf respectively. The SO_4^{2-} curve of pore water at HD319 site presents a convex up curve above 300 cmbsf and then basically quasilinearly decline with depth. It's similar to those metal ions (Ca^{2+}, Sr^{2+} and Mg^{2+}) concentration profiles at HD319 site, which all come from the overlying seawater. Also metal ions reached at low points at ~ 600 cmbsf where methane starts to increase sharply, indicating that SMTZ at HD319 is around ~ 600 cmbsf. Methane seepage provides nutrient components for anaerobic methanotrophic archaea and associated sulfate-reducing bacteria in marine sediments. The ascending methane is largely consumed at the SMTZ, producing peak concentration of DIC and total alkalinity by AOM-SR (Hu et al., 2019). In methane seep environments, pore water concentration depth profiles in shallow sediments often exhibit negative anomalies of Ca^{2+}, Mg^{2+} and Sr^{2+} concentrations, and these concentration changes can be used to identify the mineralogy of the carbonate which has currently precipitated from solution (Nöthen and Kasten, 2011). The rapid consumption of Ca^{2+}, Mg^{2+} and Sr^{2+} (Figure 2) and pore water Sr^{2+}/Ca^{2+} and Mg^{2+}/Ca^{2+} weight ratios increase within SMTZ in HD319 are most likely due to high-Mg calcite precipitation (Mazzini et al., 2006). In the present study, distinctly shallower SMTZs are observed at the ~400-800 cmbsf, which may further support high Mg-calcite precipitation in shallow sediments of four study sites in Taixinan Basin. This observation confirms that these sites are affected by methane intensities and the AOM process increases sulfate consumption, resulting in the net (production or consumption) of the main components in pore water.

Although Borowski et al. (Borowski et al., 1996; Borowski et al., 1999) showed that the change of sulfate content was mainly affected by AOM, the change of organic matter content in sediment had little effect on the gradient of sulfate concentration. Attentively, there is still sulfate concentration at the bottom of GC-10, GC-9, GC-11 and HD319 sites in Taixinan Basin, indicating that sedimentary columns contain a transition zone where methane and sulfate coexist, which is attributed to the kinetic factors of active intermediates involved in sulfide reoxidation back to sulfate (Dale et al., 2009; Holmkvist et al., 2011). Therefore, the anaerobic oxidation of methane consumes sulfate, with a stoichiometry of 1:1, thereby competing with OSR. Methane concentration gradients below the SMTZ can be used to estimate AOM rates, while sulfate concentration gradient entering SMTZ can be used to estimate sulfate reaction rate. The risk of underestimating AOM rates exists by using methane concentration gradients due to the rapid decrease in pressure. Nevertheless, in order to avoid the factors of methane escape as much as possible, studies of only some sites from limited area of the South China Sea have carefully reported methane concentration data, our GC-10, GC-9, GC-11 and HD319 sites included. Consequently, the attempt to use methane concentration gradients to constrain AOM rates is still common in the South China Sea (Chen et al., 2017; Hu et al., 2020). In all the sites from Taixinan Basin, obvious discrepancy between sulfate fluxes and methane fluxes calculated from Fick's first law are shown in Figure 2. Based on fluxes of sulfate and methane, it can be seen that the values of methane flux are always lower than those of total sulfate reduction of sulfate diffusive flux. In contrast to previous studies in similar environments, OSR was not negligible. It can be seen that the steeper the sulfate concentration gradient, the lower the sulfate reduction rate and the smaller the methane flux. This is consistent with the conclusion that methane flux plays an important role in controlling sulfate consumption in the previous study of cold seep areas (Borowski et al., 2000; Yang et al., 2010; Wu et al., 2013), and also indirectly shows the reliability of our calculation results. Therefore, it can be said that sulfate consumption is not only due to AOM in seep sediments affected by methane seepage, but also probably has related to OSR buried in the sediments.

4.2 Coupled sulfur and oxygen isotope compositions of sulfate

MSR process is characterized by complex multi-step evolution (Gilad et al., 2013) (Figure 4). First sulfate-reducing bacteria ingest sulfate and the sulfate is activated with adenosine triphosphate (ATP) to form Adenosine 5' Phosphosulfate (APS); next, the APS is reduced to SO_3^{2-}, and finally the SO_3^{2-} is reduced to H_2S and eliminate it from their cells. The S isotope fractionation effect ($\epsilon^{34}S = \delta^{34}SSO4 - \delta^{34}SH2S$) generated in MSR process mainly depends on two factors: (1) the original sulfur isotope ratio of reactants participating in each reaction step; and (2) the degree of each reversible reaction also plays a key role, due to all reactions occurring in cells are reversible during those series of processes (Rees, 1973; Brunner et al., 2005; Gilad et al., 2013; Gilad et al., 2014). During MSR (including OSR and AOM-SR), sulfate-reducing bacteria selectively preferentially ingest the lighter ^{32}S in sulfate, resulting in obvious sulfur isotope fractionation. This reaction forms H_2S with lower ^{34}S isotope values, resulting in the residual sulfate with higher ^{34}S isotope values (Canfield, 2001; Böttcher et al., 2006; Deusner et al., 2014). In addition, previous studies also noted a relationship between the magnitude of the sulfur isotope fractionation and the sulfate reduction rate (Aharon and Fu, 2000; Stam et al., 2011; Gilad et al., 2013; Bradbury et al., 2021; Chen et al., 2022). In all these studies, higher sulfur isotope fractionation corresponded to slower sulfate reduction rates.

To better understand the control mechanisms affecting two MSR processes (OSR, AOM-SR), this study further analyzed S and O isotopes ($\delta^{18}O_{SO4}$ vs. $\delta^{34}S_{SO4}$) of dissolved sulfate at C9 and C14 in

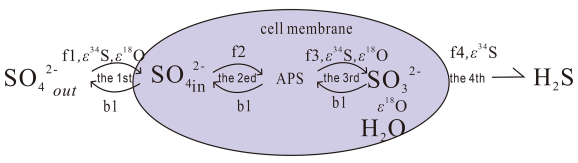

FIGURE 4
Schematic diagram showing the steps during the bacterial sulfate reduction. Arrows fi (i=1,2,3) represent the forward reaction while bi (i=1,2,3) represent the backward reactions during this process. $\epsilon^{34}s$ and $\epsilon^{18}o$ are isotope fractionation effects for sulfur and oxygen. Modified after (Fotherby et al., 2021).

Qiongdongnan basin. $\delta^{18}O_{SO4}$ and $\delta^{34}S_{SO4}$ increase fastest with sediment depth above 400 cmbsf and slowest below that depth (Figures 5A, B). They increase linearly from close to the seawater values [$\delta^{34}S_{SO4}$ = +21.24‰, (Tostevin et al., 2014); $\delta^{18}O_{SO4}$ = +8.7‰, (Johnston et al., 2014)]. Over the two sites there is a similar increase in $\delta^{18}O_{SO4}$ and $\delta^{34}S_{SO4}$; as mentioned above this slope has been linked to the overall cell-specific rate of MSR, suggesting a similar rate in sediments above 400 cmbsf. However, there is a different rate in sediments below 400 cmbsf at C9 and C14. It appears that $\delta^{34}S_{SO4}$ may increase slightly faster than $\delta^{18}O_{SO4}$ at C14 site. Moreover, we noted that the cross plot of $\delta^{18}O_{SO4}$ vs. $\delta^{34}S_{SO4}$ comes out of the apparent linear phase (Figure 5B: The pink shadow area), where the $\delta^{18}O_{SO4}$ values change slowly as the $\delta^{34}S_{SO4}$ values continue to increase. As for C9 site, the $\delta^{18}O_{SO4}$ and $\delta^{34}S_{SO4}$ values covary, and into the equilibration phase (Figure 5B: The gray shadow area).

According to the above discussion, the relative enrichment of $\delta^{18}O_{SO4}$ and $\delta^{34}S_{SO4}$ values is affected by different sulfate reduction rates and reaction mechanisms (such as OSR and AOM). The faster the sulfate reduction rate, the more constrained the O exchange process between the sulfur intermediate (SO_3^{2-}) and the surrounding water intracellularly (H_2O), resulting in an enrichment of O isotopes less than that of S isotopes. Therefore, the slope of the S-O isotope growth curve appears lower in the $\delta^{18}O_{SO4}/\delta^{34}S_{SO4}$ ratios mapping below 400 cmbsf (Figure 5) (Böttcher et al., 1998; Aharon and Fu, 2000; Gilad et al., 2013; Gilad et al., 2014). Predecessors (Gilad et al., 2014; Tostevin et al., 2014; Antler et al., 2015; Chen et al., 2022) compared and analyzed the pore water data of strong methane seeps (methane in excess) and in typical sedimentary environments (methane diffusion limited). They found that the slope of the sulfate S-O isotope curve in cold seeps ($\delta^{18}O_{SO4}/\delta^{34}S_{SO4}$ ratio) is far lower than the normal sedimentary environment, so it can be used to indicate whether the sedimentary environment is rich in methane fluids.

Take C14 site as an example, the steep slope is consistent with a normal sedimentary environment above 400 cmbsf (Figure 5B), further illustrating the primary role of OSR. Based on previous research results, it can be said that H_2S is produced during MSR or simple sulfide and other sulfur intermediates in the sediments occur, reoxidation of sulfide occurs and is disproportionation to reproduce sulfate again, accompanied by O isotope exchange with water intracellularly, resulting in significant positive correlations of $\delta^{18}O_{SO4}$ vs. $\delta^{34}S_{SO4}$ (Thamdrup et al., 1993; Böttcher et al., 2001; Chen et al., 2022). Although the $\delta^{18}O_{SO4}$ and $\delta^{34}S_{SO4}$ values below 400 cmbsf are similar to the isotope model in the methane diffusion environment (Figure 5B) (Gilad et al., 2014; Antler et al., 2015; Chen et al., 2022), the O isotopes of pore water sulfate do not significantly change with depth. Balci et al. (2007) suggested that the sulfate formed by the oxidation of pyrites in the sediment under the aerobic environment has a relatively stable O isotope value (about 5 ‰). Besides, if iron oxides are encountered during disproportionation, the sulfate generated in this process is more enriched with ^{18}O (Böttcher et al., 2001). Therefore, it is speculated that the constraint of $\delta^{18}O_{SO4}$ vs. $\delta^{34}S_{SO4}$ below 400 cmbsf at C14 may be dominated by OSR and AOM-SR. Faster MSR limits the exchange of O atoms between sulfur intermediates and the surrounding water intracellularly, and inhibits the growth of O isotopes. This conclusion indicates that in the recession or dormancy period of methane seepage, organic matter and residual methane fluids may jointly constraint the consumption of sulfate in pore water.

The two sites C9 and C14 in Qiongdongnan basin, have a large difference in the apparent sulfur isotope fractionation as evidenced by the change in $\delta^{34}S_{SO4}$; often when using the change in the isotopic composition of pore fluid to resolve the sulfur isotope fractionation factor during MSR, Rayleigh distillation is used (Rudnicki et al., 2001; Breukelen and Prommer, 2008). When the apparent sulfur isotope fractionation is calculated using this simple closed-system Rayleigh fractionation approach, significantly different sulfur isotope fractionation factors are calculated for sites C9 and C14 (Figure 6; C14 at -32‰ and C9 at -44.5‰). This feature may be related to

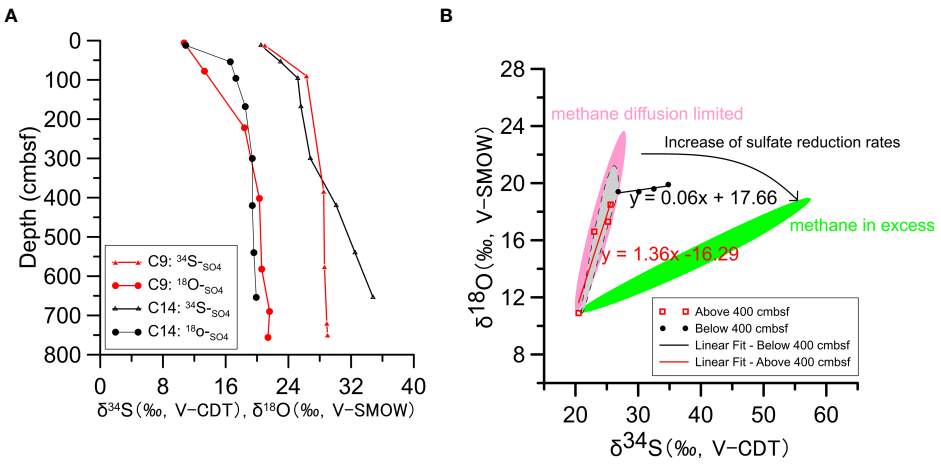

FIGURE 5
(A) S and O isotopic composition of sulfate in pore water at stations C9 and C14. **(B)** The $\delta^{18}O_{sulfate}$ versus $\delta^{34}S_{sulfate}$ data from pore water sulfate for studies sites. The lines represent the general increasing trends of pore water sulfate in a $\delta^{18}O_{sulfate}$ versus $\delta^{34}S_{sulfate}$ plot, which are based on the environmental pore water data. The pink and green shadows for "methane diffusion limited" and "methane in excess" environments, while the gray shadow for possible trend of $\delta^{18}O_{sulfate}$ versus $\delta^{34}S_{sulfate}$ at station C9.

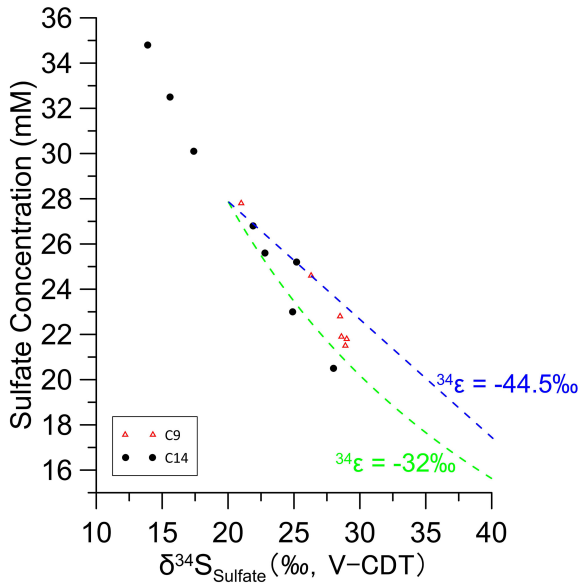

FIGURE 6
The increase in the sulfur isotope composition of sulfate as a function of the decrease in pore fluid sulfate concentrations.

different MSR processes at the bottom of the two sites. The deeper part of C14 is related to weak methane seepage, which accelerates the MSR rate. On the contrary, with the higher sulfate reduction rate at C14 site, metabolizable organic matter and weakly diffusion methane has a more significant impact on the apparent or observed sulfur isotope fractionation. Whereas the lower rate of OSR at C9 site may lower the impact methane diffusion has on the apparent evolution of the sulfur isotopic composition of the pore fluid.

In conclusion, the sulfur and oxygen isotope compositions of sulfate in pore water show that in addition to the oxidation of H_2S and the disproportionation of S intermediates, organoclastic sulfate reduction also play an important role in sulfur isotope fractionation. Evidence from Rayleigh fractionation approach shows that the sulfur and oxygen isotopes in the residual sulfate pool between organoclastic sulfate reduction and anaerobic oxidation of methane are significantly different, which are mainly affected by sulfate reduction rate and sulfur disproportionation in different degrees. These results highlight a role for organic matter during microbial sulfate reduction in cold seeps.

4.3 Influence of methane seepages on MSR

The results showed that most of the sulfate in the study area is consumed in the SMTZ, and all SMTZs except the C9 station are shallow (600-800 cmbsf). Studies by Jiang et al. (2005), Fang and Chu (2008), Yang et al. (2010) and suggested that the SMTZ position in the northern South China Sea is about 10 mbsf. The SMTZs in this study are consistent with previous studies (Borowski et al., 1996; Borowski et al., 2000; Wu et al., 2013; Miao et al., 2022). These shallow SMTZ indicate that there are relatively stable high fluxes of methane in the sediment, which enables the mutual consumption of sulfate and methane to continue. AOM existence sustained by intense methane seepages in the cold seep sediments, which may be affected by decomposition of the underlying natural gas hydrates (Liu et al., 2012). Recent studies have shown that methane seepage flux is unstable in both time and space, and is closely related to the decomposition and reformulation of natural gas hydrates (Teichert et al., 2003; Lin et al., 2016). Zhang et al. (2019) used the reaction transport model to study the spatial distributions of different biogeochemical processes in different sea areas of the South China Sea, which showed that methane flux was unevenly distributed and the rate of organic matter degradation in Qingdongnan basin was slightly higher than those in the Taixinan area. This may be related to underlying gas hydrates (Wu et al., 2013). All of this seem that OSR did occur in our sediments. The discrepancy in fluxes of sulfate and methane calculated from Fick's first law also supports occurrence of OSR at our study sites. Previous studies also showed that the ratio of sulfate flux to methane flux in SMTZ is 1.4:1 rather than 1:1. This means that about 40% of sulfate in SMTZ is consumed through OSR (Berelson et al., 2005; Lin et al., 2017; Egger et al., 2018).

A simplified model (Figure 7) shows how microbial sulfate reduction (OSR and AOM-SR) affects sulfur and oxygen isotope compositions of residual sulfate in pore water. (a) In a marine sedimentary environment, the reaction process dominated by OSR controls the stable growth and change in the S and O isotopes in residual sulfate. In addition to the OSR process with organic matter as the matrix, H_2S re-oxidation and biological disproportionation also play an essential role in the sulfur fractionation, thus accelerating the exchange of oxygen isotopes in the reaction process, leading to the rapid growth of O isotopes. (b) With low levels of methane, the sulfur and oxygen isotopes in the residual sulfate pool are controlled by the combined OSR and AOM-SR. Due to weak anaerobic oxidation of methane, sulfate reduction rate is slower and the sulfur disproportionation is significant at sulfate-methane transition zone. (c) During strong methane seepages, microbial sulfate reduction in sediments is mainly controlled by intense anaerobic oxidation of methane, but there is a certain relationship with organic matter metabolism process. The intense AOM results in a faster sulfate reduction rate and a less degree fractionation of sulfur and oxygen isotopes. In conclusion, the S and O isotopic enrichment relationship of sulfate in pore water can effectively judge and study different biogeochemical processes in sediments. In particular, it is necessary to distinguish different MSR mechanisms affected by intensity of methane seepages. Nonetheless, to what extent the impact of organic matter from cold seep sediments on the S and O isotopes in residual sulfate remains to be investigated.

5 Conclusions

This paper used pore water data combined with PROFILE model and fluxes of methane and sulfate in Qiongdongnan and Taixinan basins to conduct a geochemical study of the sites to further clarify miarobial sulfate reduction process related to OSR and AOM-SR under the background of methane seepages. Our results suggest that SMTZ positions in all study sites are roughly ~600 to 800 cmbsf,

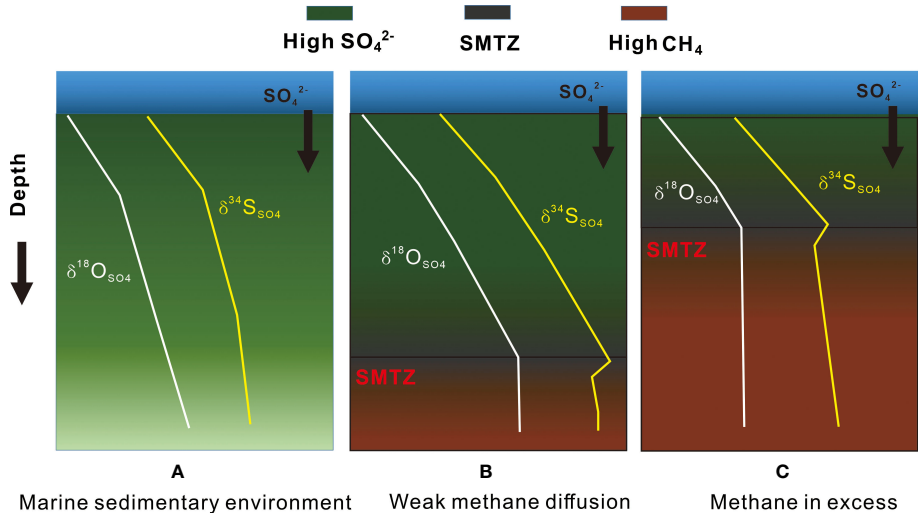

FIGURE 7
Variations of $\delta^{18}O_{SO4}$ and $\delta^{34}S_{SO4}$ with depth. **(A)** represents the normal marine sedimentary environment without methane impact; **(B)** represents the sedimentary environment with weak methane diffusion; **(C)** represents the sedimentary environment with methane in excess.

which is relatively shallower compared to international SMTZs in cold seeps. The values of methane flux are always lower than those of total sulfate reduction of sulfate diffusive flux. Combined with $\delta^{34}S_{SO4}$ vs. $\delta^{18}O_{SO4}$ of residual sulfate, it can be said that the coexistence of OSR and AOM-SR in methane seep sediments in Qiongdongnan. Beyond the intensity of methane seepages, the presence of OSR to a greater extent results in affecting the microbial sulfate reduction rate, and thus causing fractionation of sulfur and oxygen isotopes in residual sulfate pool. This emphasizes that the traditional redox order of bacterial respiration is highly simplified, where, in sediments such as these seeps, all of these processes can occur together with complex couplings between them. Nonetheless, further studies remain to be investigated.

Data availability statement

The datasets presented in this study can be found in online repositories. The names of the repository/repositories and accession number(s) can be found in the article/Supplementary Material.

Author contributions

TS designed and wrote the manuscript and analyzed the modeled data related to the pore water. DW designed the study and provided pore water data in Taixinan Basin. PY and NW helped to revise the manuscript and give some useful suggestions. All authors contributed to the article and approved the submitted version.

Funding

This work was financially supported by the Postdoctoral Foundation of Qingdao (Grant QDBSH20220202138), the China Geological Survey Project (NO. DD20190276) and the Fund of Ministry of Science and Technology (Nos 2013FY112200 and 2019YFE0127200).

Acknowledgments

We are grateful to the editors and reviewers for their constructive comments on our manuscript.

Conflict of interest

The authors declare that the research was conducted in the absence of any commercial or financial relationships that could be construed as a potential conflict of interest.

The reviewer RY declared a shared affiliation with the authors TS, NW, PY to the handling editor at the time of review.

Publisher's note

Supplementary material

The Supplementary Material for this article can be found online at: https://www.frontiersin.org/articles/10.3389/fmars.2023.1111133/full#supplementary-material

References

Aharon, P., and Fu, B. (2000). Microbial sulfate reduction rates and sulfur and oxygen isotope fractionations at oil and gas seeps in deepwater gulf of Mexico. *Geochimica Cosmochimica Acta* 64, 233–246. doi: 10.1016/S0016-7037(99)00292-6

Antler, G., Turchyn, V., Herut, B., and Sivan, O. (2015). A unique isotopic fingerprint of sulfate-driven anaerobic oxidation of methane. *Geology* 43 (7), 619–622. doi: 10.1130/G36688.1

Balci, N., Shanks, W., Mayer, B., and Mandernack, K. (2007). Oxygen and sulfur isotope systematic of sulfate produced by bacterial and abiotic oxidation of pyrite. *Geochimica Cosmochimica Acta* 71, 3796–3811. doi: 10.1016/j.gca.2007.04.017

Berelson, W., Prokopenko, M., Sansone, F., Graham, A., McManus, J., and Bernhard, J. (2005). Anaerobic diagenesis of silica and carbon in continental margin sediments: Discrete zones of TCO_2 production'. *Geochimica Cosmochimica Acta* 69, 4611–4629. doi: 10.1016/j.gca.2005.05.011

Berg, P., Risgaard-Petersen, N., and Rysgaard, Søren (1998). Interpretation of measured concentration profiles in sediment pore water. *Limnol. Oceanogr.* 13, 395–411. doi: 10.4319/lo.1998.43.7.1500

Berner, R., de Leeuw, J., Spiro, B., Murchison, D., and Eglinton, G. (1985). Sulphate reduction, organic matter decomposition and pyrite formation [and discussion]. *Philos. Trans. R. Soc. A: Mathematical Phys. Eng. Sci.* 315, 25–38. doi: 10.1098/rsta.1985.0027

Boetius, A., Ravenschlag, K., Schubert, J.C., Rickert, D., and Widdel, F. (2000). A marine microbial consortium apparently mediating anaerobic oxidation of methane. *Nature* 407, 623–629. doi: 10.1038/35036572

Borowski, W., Paull, C., and Ussler, B. (1999). Global and local variations of interstitial sulfate gradients in deep-water, continental margin sediments: Sensitivity to underlying methane and gas hydrates. *Mar. Geology* 159, 131–154. doi: 10.1016/S0025-3227(99)00004-3

Borowski, W., Hoehler, T., Alperin, M., Rodriguez, N., and Paull, C. (2000). Significance of anaerobic methane oxidation in methane-rich sediments overlying the Blake ridge gas hydrates. *Proc. Ocean Drilling Program: Sci. Results* 164, 87–99. doi: 10.2973/odp.proc.sr.164.214.2000

Borowski, W., Paull, C., and Ussler, B. (1996). Marine pore-water sulfate profiles indicate *in situ* methane flux from underlying gas hydrate. *Geology* 24, 655–658. doi: 10.1130/0091-7613(1996)024<0655:MPWSPI>2.3.CO;2

Böttcher, M. E. (1998). Manganese (II) partitioning during experimental precipitation of rhodochrosite–calcite solid solutions from aqueous solutions. *Mar. Chem.* 62, 287–297. doi: 10.1016/S0304-4203(98)00039-5

Böttcher, M., Boetius, A., and Rickert, D. (2006). *Sulfur isotope fractionation during microbial sulfate reduction associated with anaerobic methane oxidation*. European Geosciences Union. doi: 1607-7962/gra/EGU06-A-10040

Böttcher, M. E., Brumsack, H. J., and Lange, G. (1998). Sulfate reduction and related stable isotope (^{34}S, ^{18}O) variations in interstitial waters from the Eastern Mediterranean. In A. H. F. Robertson, K.-C. Emeis, C. Richter and A. Camerlenghi *Proccedings of the Ocean Drlling Program, Leg 160.* (Eastern Mediterranean. College Station, TX: Ocean Drilling Program). 365–373. doi: 10.2973/odp.proc.sr.160.002.1998

Böttcher, M., Thamdrup, Bo, and Vennemann, T. (2001). Oxygen and sulfur isotope fractionation during anaerobic bacterial disproportionation of elemental sulfur. *Geochimica Cosmochimica Acta* 65, 1601–1609. doi: 10.1016/S0016-7037(00)00628-1

Boudreau, B. P. (1997). Diagenetic models and their implementation. *Springer*. doi: 10.1007/978-3-642-60421-8

Bradbury, H. J., Turchyn, A. V., Bateson, A., Antler, G., Fotherby, A., Druhan, J. L., et al. (2021). The carbon-sulfur link in the remineralization of organic carbon in surface sediments. *Front. Earth Sci.* 9, 652960. doi: 10.3389/feart.2021.652960

Breukelen, B., and Prommer, H. (2008). Beyond the Rayleigh equation: Reactive transport modeling of isotope fractionation effects to improve quantification of biodegradation. *Environ. Sci. Technol.* 42, 2457–2463. doi: 10.1021/es071981j

Brunner, B., Bernasconi, S., Kleikemper, J., and Schroth, M. (2005). A model for oxygen and sulfur isotope fractionation in sulfate during bacterial sulfate reduction processes. *Geochimica Cosmochimica Acta* 69, 4773–4785. doi: 10.1016/j.gca.2005.04.017

Canfield, D. (2001). Isotope fractionation by natural populations of sulfate-reducing bacteria. *Geochimica Cosmochimica Acta* 65, 1117–1124. doi: 10.1016/S0016-7037(00)00584-6

Canfield, D., Olesen, C., and Cox, R. (2006). Temperature and its control of isotope fractionation by a sulfate-reducing bacterium. *Geochimica Cosmochimica Acta* 70, 548–561. doi: 10.1016/j.gca.2005.10.028

Chen, T., Strauss, H., Fang, Y., Lin, Z., Sun, X., Liu, J., et al. (2022). Sulfur and oxygen isotope records of sulfate-driven anaerobic oxidation of methane in diffusion-dominated marine sediments. *Front. Earth Sci.* 10, 862333. doi: 10.3389/feart.2022.862333

Chen, N.-C., Yang, T. F., Hong, W.-L., Chen, H.-W., Chen, H.-C., Hu, C.-Y., et al. (2017). Production, consumption, and migration of methane in accretionary prism of southwestern Taiwan. *Geochemistry Geophysics Geosystems* 18 (8), 2970–2989. doi: 10.1002/2017GC006798

Dale, A., Regnier, P., Van Cappellen, P., Fossing, H., Jensen, Jørn, and Jørgensen, Bo (2009). Remote quantification of methane fluxes in gassy marine sediments through seismic survey. *Geology* 37, 235–238. doi: 10.1130/G25323A.1

Deusner, C., Holler, T., Arnold, G. L., Bernasconi, S. M., Formolo, M. J., and Brunner, B. (2014). Sulfur and oxygen isotope fractionation during sulfate reduction coupled to anaerobic oxidation of methane is dependent on methane concentration. *Earth Planetary Sci. Lett.* 399, 61–73. doi: 10.1016/j.epsl.2014.04.047

Egger, M., Riedinger, N., Mogollón, J., and Jørgensen, Bo (2018). Global diffusive fluxes of methane in marine sediments. *Nat. Geosci.* 11, 421–425. doi: 10.1038/s41561-018-0122-8

Fang, Y., and Chu, F. (2008). The relationship of sulfate-methane interface,the methane flux and the underlying gas hydrate. *Mar. Sci. Bull.* 10, 28–37.

Fotherby, A., Bradbury, H., Antler, G., Sun, X., Druhan, J., and Turchyn, A. (2021). Modelling the effects of non-steady state transport dynamics on the sulfur and oxygen isotope composition of sulfate in sedimentary pore fluids. *Front. Earth Sci.* 8. doi: 10.3389/feart.2020.587085

Gilad, A., Turchyn, A., Herut, B., Davies, A., Rennie, V., and Sivan, O. (2014). Sulfur and oxygen isotope tracing of sulfate driven anaerobic methane oxidation in estuarine sediments. *Estuarine Coast. Shelf Sci.* 142, 4–11. doi: 10.1016/j.ecss.2014.03.001

Gilad, A., Turchyn, A., Rennie, V., Herut, B., and Sivan, O. (2013). Coupled sulfur and oxygen isotope insight into bacterial sulfate reduction in the natural environment. *Geochimica Cosmochimica Acta* 118, 98–117. doi: 10.1016/j.gca.2013.05.005

Han, X., Suess, E., Huang, Y., Wu, N., Bohrmann, G., Su, X., et al. (2008). Jiulong methane reef: Microbial mediation of seep carbonates in the south China Sea. *Mar. Geology* 249, 243–256. doi: 10.1016/j.margeo.2007.11.012

Holmkvist, L., Kamyshny, A., Vogt, C., Vamvakopoulos, K., Ferdelman, T., and Jørgensen, Bo (2011). Sulfate reduction below the sulfate–methane transition in black Sea sediments. *Deep Sea Res. Part I: Oceanographic Res. Papers* 58, 493–504. doi: 10.1016/j.dsr.2011.02.009

Hu, Yu, Feng, D., Liang, Q., Xia, Z., Chen, L., and Chen, D. (2015). Impact of anaerobic oxidation of methane on the geochemical cycle of redox-sensitive elements at cold-seep sites of the northern south China Sea. *Deep Sea Res. Part II: Topical Studies in Oceanography* 122, 84–94. doi: 10.1016/j.dsr2.2015.06.012

Hu, Y., Feng, D., Peckmann, J., Gong, S., Liang, Q., Wang, H., et al. (2020). The impact of diffusive transport of methane on pore-water and sediment geochemistry constrained by authigenic enrichments of carbon, sulfur, and trace elements: A case study from the shenhu area of the south China Sea. *Chem. Geology* 553, 119805. doi: 10.1016/j.chemgeo.2020.119805

Hu, Y., Liang, Q., Chen, L., Feng, D., Yang, S., Liang, J., et al. (2019). Pore fluid compositions and inferred fluid flow patterns at the haima cold seeps of the south China Sea. *Mar. Petroleum Geology* 103, 29–40. doi: 10.1016/j.marpetgeo.2019.01.007

Iversen, N., and Jørgensen, B. (1993). Diffusion coefficients of sulfate and methane in marine sediments: Influence of porosity. *Geochimica Cosmochimica Acta* 57, 571–578. doi: 10.1016/0016-7037(93)90368-7

Jørgensen, N. (1992). Methane-derived carbonate cementation of Holocene marine sediments from kattegat, Denmark. *Continental Shelf Res.* 12, 1209–1218. doi: 10.1016/0278-4343(92)90080-4

Jørgensen, B., Beulig, F., Egger, M., Petro, C., Scholze, C., and Røy, H. (2019b). Organoclastic sulfate reduction in the sulfate-methane transition of marine sediments. *Geochimica Cosmochimica Acta* 254, 231–245. doi: 10.1016/j.gca.2019.03.016

Jørgensen, Bo B., Böttcher, M. E., Lüschen, H., Neretin, L. N., and Volkov., I. I. (2004). Anaerobic methane oxidation and a deep H2S sink generate isotopically heavy sulfides in black Sea sediments. *Geochimica Cosmochimica Acta* 68, 2095–2118. doi: 10.1016/j.gca.2003.07.017

Jørgensen, Bo B., Findlay, A. J., and Pellerin, André (2019a). The biogeochemical sulfur cycle of marine sediments. *Front. Microbiol.* 10, 1–27. doi: 10.3389/fmicb.2019.00849

Jørgensen, Bo B., Weber, A., and Zopfi, J. (2001). 'Sulfate reduction and anaerobic methane oxidation in black Sea sediments. *Deep Sea Res. Part I: Oceanographic Res. Papers* 48, 2097–2120. doi: 10.1016/S0967-0637(01)00007-3

Jiang, S. Y., Yang, T., Xue, Z. C., Yang, J. H., Ling, H. F., Wu, N., et al. (2005). Chlorine and sulfate concentrations in pore waters from marine sediments in the north margin of the south China Sea and their implications for gas hydrate exploration. *Geoscience* 19 (1), 45–54. doi:1000-8527(2005)01-0045-10

Jin, C., and Wang, J. (2010). A preliminary study of the gas hydrate stability zone in the south China Sea. *Acta Geologica Sinica-English Edition* 76, 423–428. doi: 10.1111/j.1755-6724.2002.tb00095.x

Johnston, D. T., Gill, B. C., Masterson, A., Beirne, E., Casciotti, K. L., Knapp, A. N., et al. (2014). Placing an upper limit on cryptic marine sulphur cycling. *Nature* 513, 530–533. doi: 10.1038/nature13698

Knittel, K., and Boetius, A. (2009). Anaerobic oxidation of methane: Progress with an unknown process. *Annu. Rev. Microbiol.* 63, 311–334. doi: 10.1146/annurev.micro.61.080706.093130

Liang, Q., Hu, Y., Feng, D., Peckmann, J., Chen, L., Yang, S., et al. (2017). Authigenic carbonates from newly discovered active cold seeps on the northwestern slope of the south China Sea: Constraints on fluid sources, formation environments, and seepage dynamics. *Deep Sea Res. Part I: Oceanographic Res. Papers* 124, 31–41. doi: 10.1016/j.dsr.2017.04.015

Lin, Z., Lu, Y., Xu, L., Gong, J., Lu, H., Teichert, B., et al. (2016). Stable isotope patterns of coexisting pyrite and gypsum indicating variable methane flow at a seep site of the shenhu area, south China sea'. *J. Asian Earth Sci.* 123, 213–223. doi: 10.1016/j.jseaes.2016.04.007

Lin, Z., Strauss, H., Lu, Y., Gong, J., Xu, L., Lu, H., et al. (2017). Multiple sulfur isotope constraints on sulfate-driven anaerobic oxidation of methane: Evidence from authigenic pyrite in seepage areas of the south China Sea. *Geochimica Cosmochimica Acta* 211, 153–173. doi: 10.1016/j.gca.2017.05.015

Liu, C., Ye, Y., Meng, Q.-G., He, X., Lu, H., Zhang, J., et al. (2012). The characteristics of gas hydrates recovered from shenhu area in the south China Sea. *Mar. Geology* 307-310, 22–27. doi: 10.1016/j.margeo.2012.03.004

Luo, M., Chen, L., Tong, H., Yan, W., and Chen, D. (2014). Gas hydrate occurrence inferred from dissolved cl– concentrations and δ18O values of pore water and dissolved sulfate in the shallow sediments of the pockmark field in southwestern xisha uplift, northern south China Sea. *Energies* 7, 3886–3899. doi: 10.3390/en7063886

Luo, M., Chen, L., Wang, S., Yan, W., Wang, H., and Chen, D. (2013). Pockmark activity inferred from pore water geochemistry in shallow sediments of the pockmark field in southwestern xisha uplift, northwestern south China Sea. *Mar. Petroleum Geology* 48, 247–259. doi: 10.1016/j.marpetgeo.2013.08.018

Malinverno, A., and Pohlman, J. (2011). Modeling sulfate reduction in methane hydrate-bearing continental margin sediments: Does a sulfate-methane transition require anaerobic oxidation of methane? *Geochemistry Geophysics Geosystems* 12, 1525–2027. doi: 10.1029/2011GC003501

Masuzawa, T., Handa, N., Kitagawa, H., and Kusakabe, M. (1992). Sulfate reduction using methane in sediments beneath a bathyal "cold seep" giant clam community off hatsushima island, sagami bay, Japan. *Earth Planetary Sci. Lett.* 110, 39–50. doi: 10.1016/0012-821X(92)90037-V

Mazzini, A., Henrik, S., Martin, H., and Sverre, P. (2006). Comparison and implications from strikingly different authigenic carbonates in a Nyegga complex pockmark, G11, Norwegian Sea. *Marine Geology* 231, 89–102.

Miao, X., Liu, X., Li, Q., Li, A., Cai, F., Kong, F., et al. (2022). Porewater geochemistry indicates methane seepage in the Okinawa Trough and its implications for the carbon cycle of the subtropical West Pacific. *Palaeogeogr. Palaeoclimatol. Palaeoecol.* 607, 111266. doi: 10.1016/j.palaeo.2022.111266

Nöthen, K., and Sabine, K. (2011). Reconstructing changes in seep activity by means of pore water and solid phase Sr/Ca and Mg/Ca ratios in pockmark sediments of the Northern Congo Fan. *Marine Geology* 287, 1–13.

Pellerin, A., Gilad, A., Holm, S., Findlay, A., Crockford, P., Turchyn, A., et al. (2019). Large Sulfur isotope fractionation by bacterial sulfide oxidation. *Sci. Adv.* 5 (7), 1–6. doi: 10.1126/sciadv.aaw1480

Piker, L., Schmaljohann, R., and Imhoff, J. (1998). Dissimilatory sulfate reduction and methane production in gotland deep sediments (Baltic Sea) during a transition period from oxic to anoxic bottom water. *Aquat. Microbial Ecol.* 14, 183–193. doi: 10.3354/ame014183

Reeburgh, W. S. (1976). Methane consumption in cariaco trench waters and sediments. *Earth Planetary ence Lett.* 28, 337–344. doi: 10.1016/0012-821X(76)90195-3

Rees, C. E. (1973). Steady-state model for sulfur isotope fractionation in bacterial reduction processes. *Geochimica Cosmochimica Acta* 37, 1141–1162. doi: 10.1016/0016-7037(73)90052-5

Rudnicki, M., Elderfield, H., and Spiro, B. (2001). Fractionation of sulfur isotopes during bacterial sulfate reduction in deep ocean sediments at elevated temperatures. *Geochimica Cosmochimica Acta* 65, 777–789. doi: 10.1016/S0016-7037(00)00579-2

Santos, A., Venceslau, S., Grein, F., Leavitt, W., Dahl, C., Johnston, D., et al. (2015). A protein trisulfide couples dissimilatory sulfate reduction to energy conservation. *Science* 350 (6267), 1541–1545. doi: 10.1126/science.aad3558

Schmaljohann, R. (1996). Methane dynamics in the sediment and water column of Kiel harbour (Baltic Sea). *Mar. Ecology-progress Ser.* 131, 263–273. doi: 10.3354/meps131263

Schnürle, P., Liu, C.-S., Lin, A. T., and Lin, S. (2011). Structural controls on the formation of BSR over a diapiric anticline from a dense MCS survey offshore southwestern Taiwan. *Mar. Petrol. Geol.* 28 (10), 1932–1942. doi: 10.1016/j.marpetgeo.2010.12.004

Schulz, H. D. (2006). "Quantification of early diagenesis: dissolved constituents in pore water and signals in the solid phase," in *Marine geochemistry* (Springer).

Shi, W., Xie, Y., Wang, Z., Li, X., and Tong, C. (2013). Characteristics of overpressure distribution and its implication for hydrocarbon exploration in the qiongdongnan basin. *J. Asian Earth Sci.* 66, 150–165. doi: 10.1016/j.jseaes.2012.12.037

Stam, M., Mason, P. R. D., Laverman, A., Pallud, C., and Van Cappellen, P. (2011). 34S/ 32S fractionation by sulfate-reducing microbial communities in estuarine sediments. *Geochimica Et Cosmochimica Acta - GEOCHIM COSMOCHIM Acta* 75, 3903–3914. doi: 10.1016/j.gca.2011.04.022

Suess, E., Huang, Y. Y., and Wu, N. (2005). "Cruise report SO177, sino-German cooperative project, south China Sea," in *Distribution, formation and effect of methane & gas hydrate on the environment*. Available at: http://store.pangaea.de/documentation/Reports/SO177.pdf.

Sun, Q., Wu, S., Hovland, M., Luo, P., Lu, Y., and Qu, T. (2011). The morphologies and genesis of mega-pockmarks near the xisha uplift, south China Sea. *Mar. Petroleum Geology* 28, 1146–1156. doi: 10.1016/j.marpetgeo.2011.03.003

Taylor, B., and Hayes, D. E. (1983). Origin and history of the south China Sea basin. *Tectonic Geologic Evol. Southeast Asian Seas Islands: Part 2* 27, 23–56. doi: 10.1029/GM027p0023

Teichert, B., Eisenhauer, A., Bohrmann, G., Haase - Schramm, A., Bock, B., and Linke, P. (2003). U/Th systematics and ages of authigenic carbonates from hydrate ridge, cascadia margin: Recorders of fluid flow variations. *Geochimica Cosmochimica Acta* 67 (20), 3845–3857. doi: 10.1016/S0016-7037(03)00128-5

Thamdrup, B. O., Finster, K., Hansen, J. Würgler, and Bak, F. (1993). Bacterial disproportionation of elemental sulfur coupled to chemical reduction of iron or manganese. *Appl. Environ. Microbiol.* 59, 101–108. doi: 10.1128/aem.59.1.101-108.1993

Tostevin, R., Turchyn, A., Farquhar, J., Johnston, D., Eldridge, D., Bishop, J., et al. (2014). Multiple sulfur isotope constraints on the modern sulfur cycle. *Earth Planetary Sci. Lett.* 396, 14–21. doi: 10.1016/j.epsl.2014.03.057

Wang, P., Prell, W. L., and Blum, P. (2000). Initial reports. *Proc. Ocean Drill. Prog.*, 184.

Wing, B., and Halevy, I. (2014). Intracellular metabolite levels shape sulfur isotope fractionation during microbial sulfate respiration. *Proc. Natl. Acad. Sci. United States America* 111, 18116–18125. doi: 10.1073/pnas.1407502111

Wu, D., Wu, N., Fu, S., Liang, J., and Guan, H. (2010). Geochemical characteristics of shallow sediments in the gas hydrate distribution area of dongsha, the northern south China Sea. *Mar. Geology Quaternary Geology* 30, 41–51.

Wu, D., Wu, N., Zhang, M., Guan, H., Fu, S., and Yang, R. (2013). Relationship of sulfate-methane tnterface (SMI), methane fluux and the underlying gas hydrate in dongsha area, northern south China Sea. *Earth Science- J. China Univ. Geosciences* 38, 1309–1320.

Yang, T., Jiang, S.-Y., Ge, L., Yang, J., Wu, N., Zhang, G., et al. (2010). Geochemical characteristics of pore water in shallow sediments from shenhu area of south China Sea and their significance for gas hydrate occurrence. *Chin. Sci. Bull.* 55, 752–760. doi: 10.1007/s11434-009-0312-2

Yao, B. (1998). Preliminary study on gas hydrate in the northern continental margin of the south china sea. *Mar. Geology Quaternary Geology* 18, 11–18. doi: 10.16562/j.cnki.0256-1492.1998.04.002

Zhang, W., Liang, J., Su, P., Wei, J., Gong, Y., Lin, L., et al. (2018). Distribution and characteristics of mud diapirs, gas chimneys, and bottom simulating reflectors associated with hydrocarbon migration and gas hydrate accumulation in the qiongdongnan basin, northern slope of the south China Sea. *Geological J.* 54, 1–18. doi: 10.1002/gj.3351

Zhang, P., Zuraida, R., Rosenthal, Y., Holbourn, A., Kuhnt, W., and Xu, J. (2019). Geochemical characteristics from tests of four modern planktonic foraminiferal species in the Indonesian throughflow region and their implications. *Geosci. Front.* 10, 505–516. doi: 10.1016/j.gsf.2018.01.011

Zhu, W., Huang, B., Mi, L., Wilkins, R., Fu, N., and Xiao, X. (2009). Geochemistry, origin and deep-water exploration potential of natural gases in the pearl river mouth and qiongdongnan basins, south China Sea. *Aapg Bull. - AAPG Bull.* 93, 741–776. doi: 10.1306/02170908099